Supplementary Document

Ensemble Number	ENS1	ENS2	ENS3	ENS4	ENS5	ENS6	ENS7	ENS8	ENS9
ENSO (DJF)	Warm	Cold	Cold	Warm	Cold	Neutral	Cold	Neutral	Warm
QBO (@30hPa)	Easterly	Easterly	Easterly	Easterly	Westerly	Easterly	Easterly	Westerly	Westerly
Ensemble Number	**ENS10**	**ENS11**	**ENS12**	**ENS13**	**ENS14**	**ENS15**	**ENS16**	**ENS17**	**ENS18**
ENSO (DJF)	Warm	Cold	Cold	Warm	Cold	Neutral	Cold	Neutral	Warm
QBO (@30hPa)	Easterly	Easterly	Easterly	Easterly	Westerly	Westerly	Easterly	Westerly	Westerly

Table S1. UKESM Ensemble Season, QBO, and ENSO Initial Phase Classifications.

Additional Explanation of QBO and ENSO Classifications

The QBO is a downward propagating quasiperiodic oscillation of the equatorial zonal wind between easterlies and westerlies in the tropical stratosphere (Baldwin et al., 2001). In this study QBO state was characterized by the wind velocity between 15°N and 15°S, across all longitudes at a pressure of 30hPa, with initial QBO state being defined at the month of eruption. Positive wind velocities denote a Westerly QBO phase with negative ones denoting an Easterly phase. This resulted in 6 easterly and 3 westerly classified July ensembles and 5 easterly and 4 westerly classified January ensembles.

The ENSO is an interannual climate variation, characterized by a cycle of anomalous winds and sea surface temperatures (SST) over the tropical eastern Pacific. The warm SST phase, coupled with weakened trade winds, is known as El Niño and the cold phase, accompanied by enhanced trade winds, as La Niña, with a neutral phase in between. In this study ENSO phase was characterized as either warm, cold, or neutral using the December-January-February (DJF) NH Winter Niño 3.4 Index, where January is the reference for the year, as done by Zanchettin et al., (2016). To classify the ensembles the spatially averaged mean DJF SST anomaly was calculated for the Niño 3.4 region (5°N-5°S, 170°W-120°W) with warm and cold phases defined when the anomalies exceed +/- 0.4°C respectively (Trenberth and Stepaniak, 2001). This resulted in 3 warm, 2 neutral, and 4 cold phase classified ensembles across both January and July ensembles.

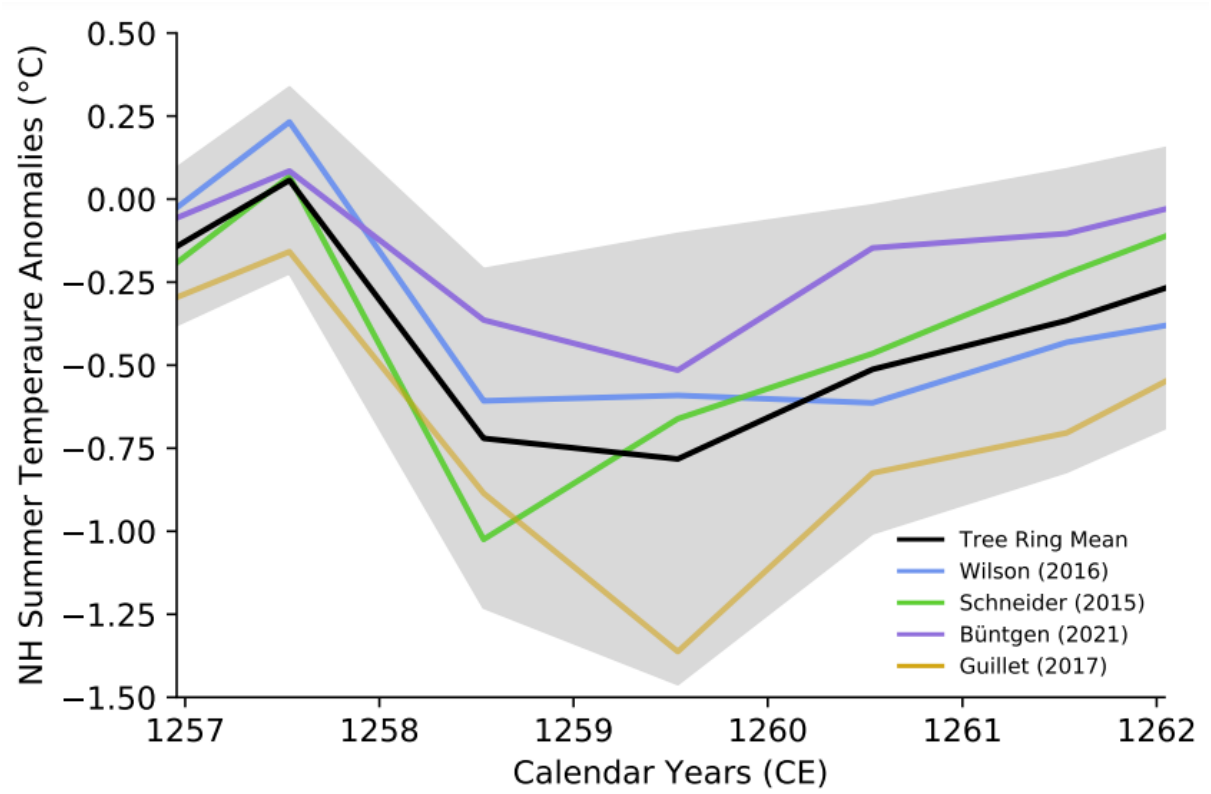

Figure S1. Northern Hemisphere Summer (June-July-August) Temperature Anomalies for Individual Tree Ring Reconstruction datasets. Black line shows the tree-ring reconstructed mean utilised in the main text Figure 1 with the grey band showing 2σ around the mean.

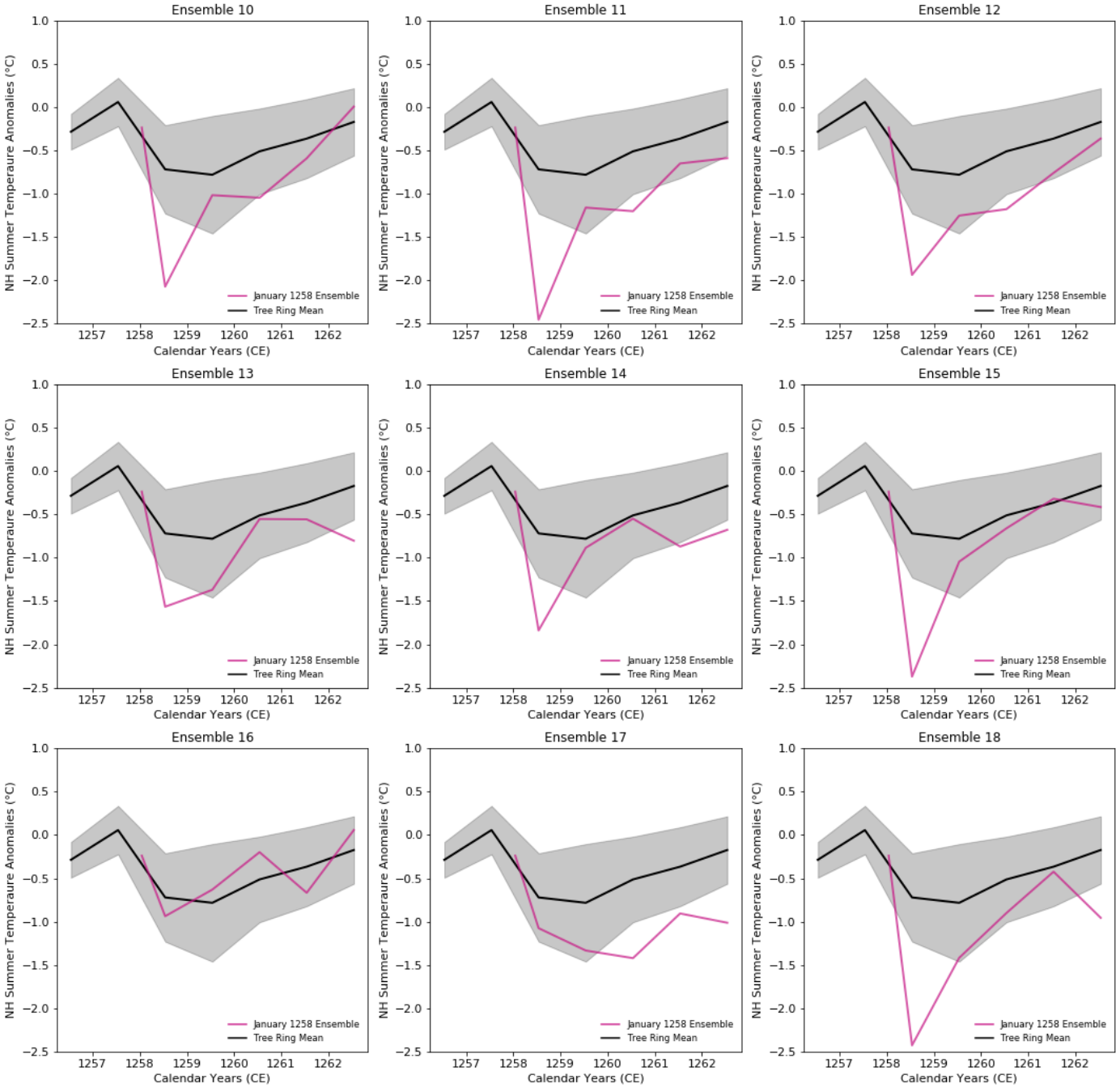

Figure S2. Model-simulated Northern Hemisphere Summer (June-July-August) Temperature Anomalies for individual January 1258 ensembles. Black line shows the tree-ring reconstructed mean with the grey band showing 2σ around the mean. Of the 9 January 1258 Ensembles only 2 lie within 2σ of the tree ring-reconstructed mean for Summer 1258.

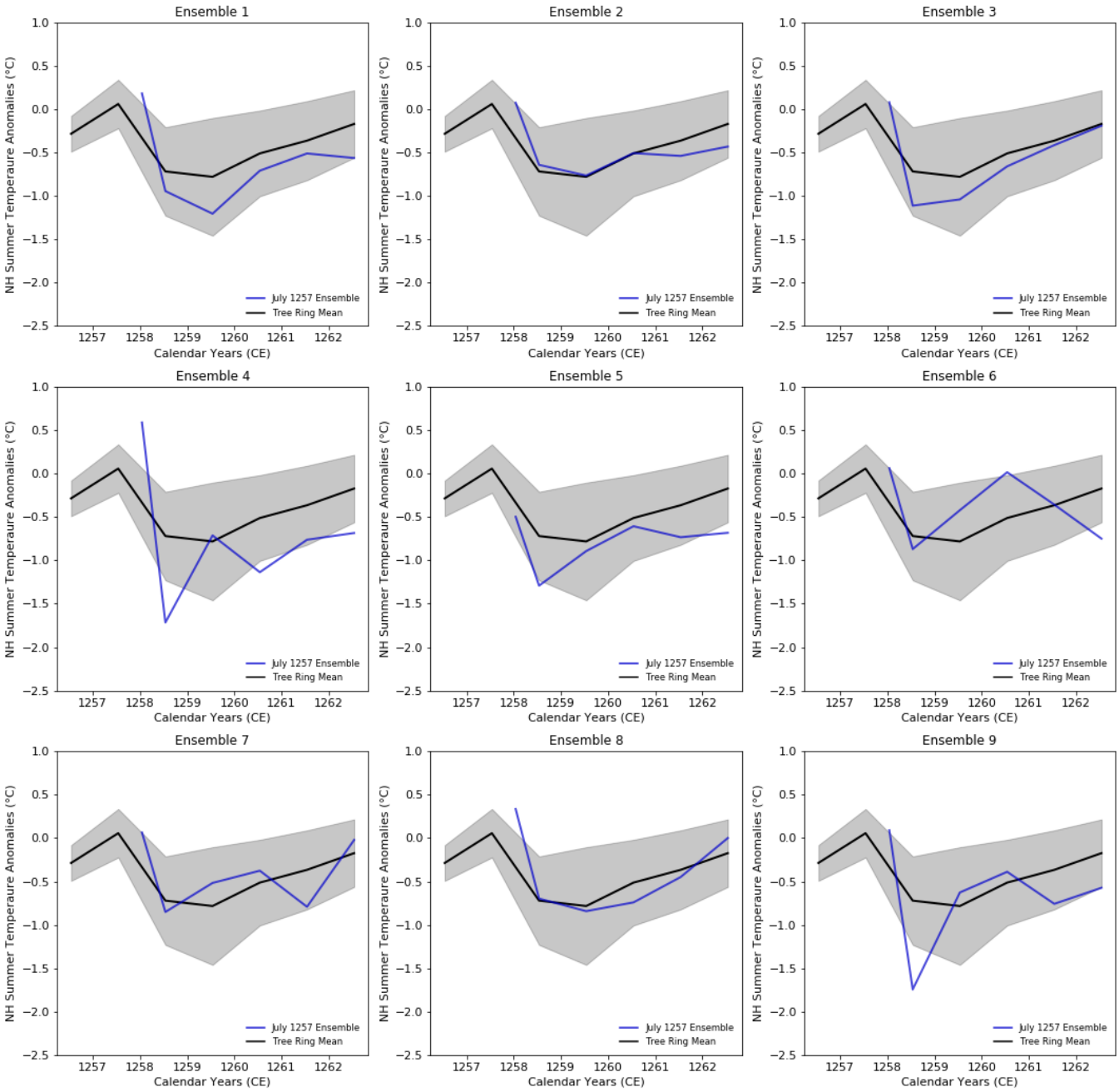

Figure S3. Model-simulated Northern Hemisphere Summer (June-July-August) Temperature Anomalies for individual July 1257 ensembles. Black line shows the tree-ring reconstructed mean with the grey band showing 2σ around the mean. Of the 9 July 1257 Ensembles 7 lie within 2σ of the tree ring-reconstructed mean for Summer 1258.

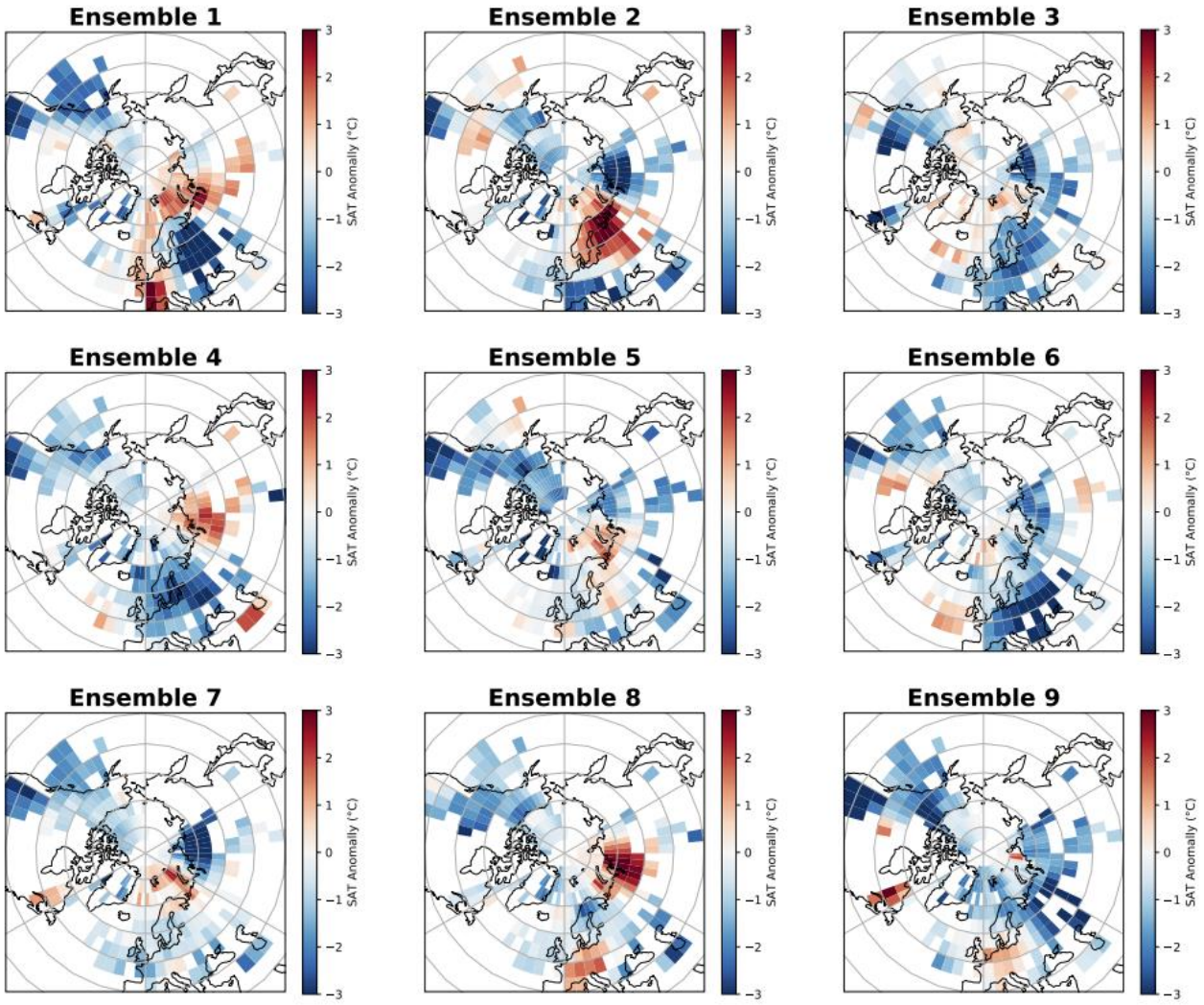

Figure S4. Spatially resolved NH Summer (JJA) Temperature Anomalies for individual July 1257 ensembles for Summer 1258. Model-simulated anomalies were regridded to be comparable to the NTREND spatially resolved dataset (Anchukaitis et al., 2017).

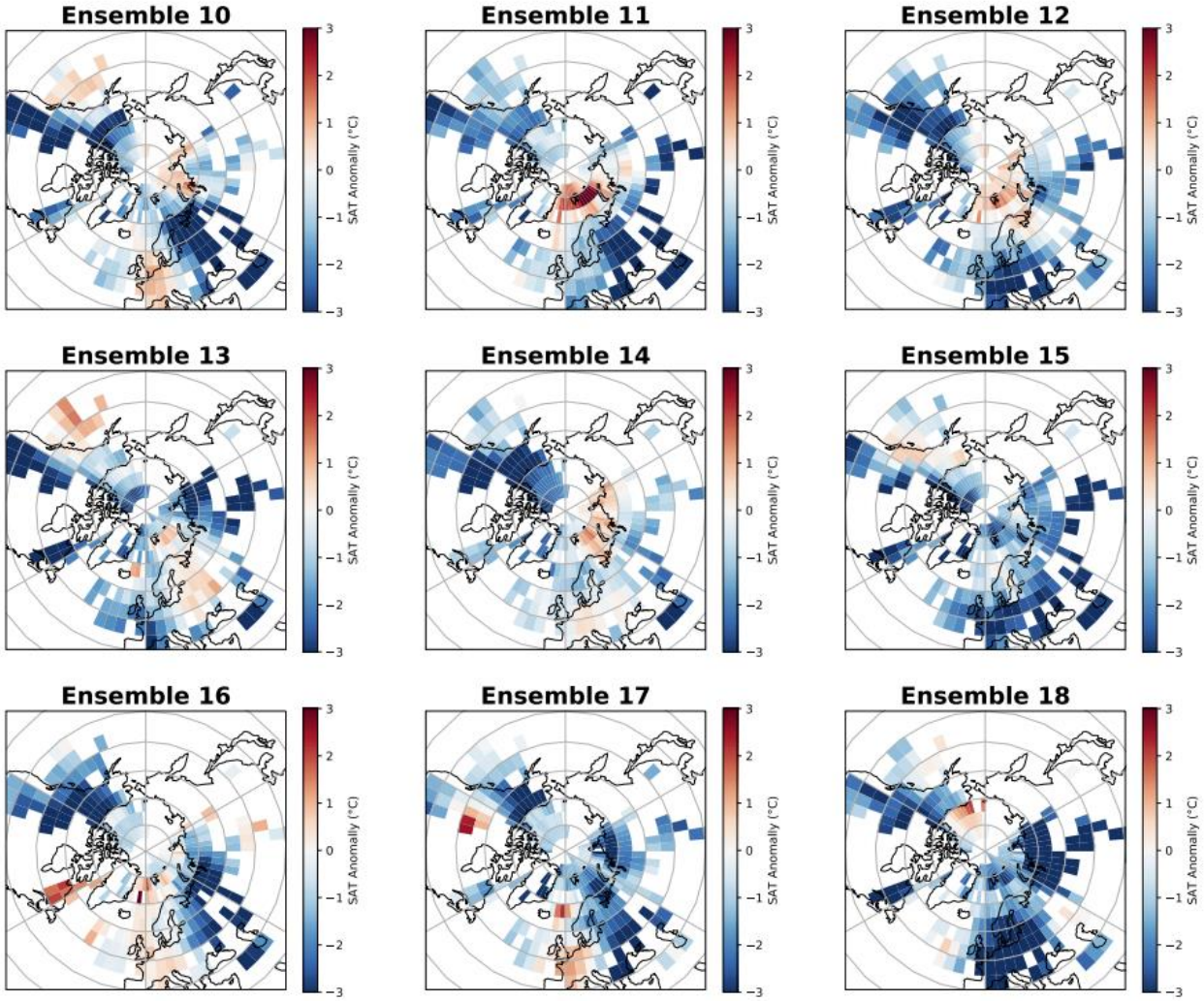

Figure S5. Spatially resolved NH Summer (JJA) Temperature Anomalies for individual January 1258 ensembles for Summer 1258. Model-simulated anomalies were regridded to be comparable to the NTREND spatially resolved dataset (Anchukaitis et al., 2017).

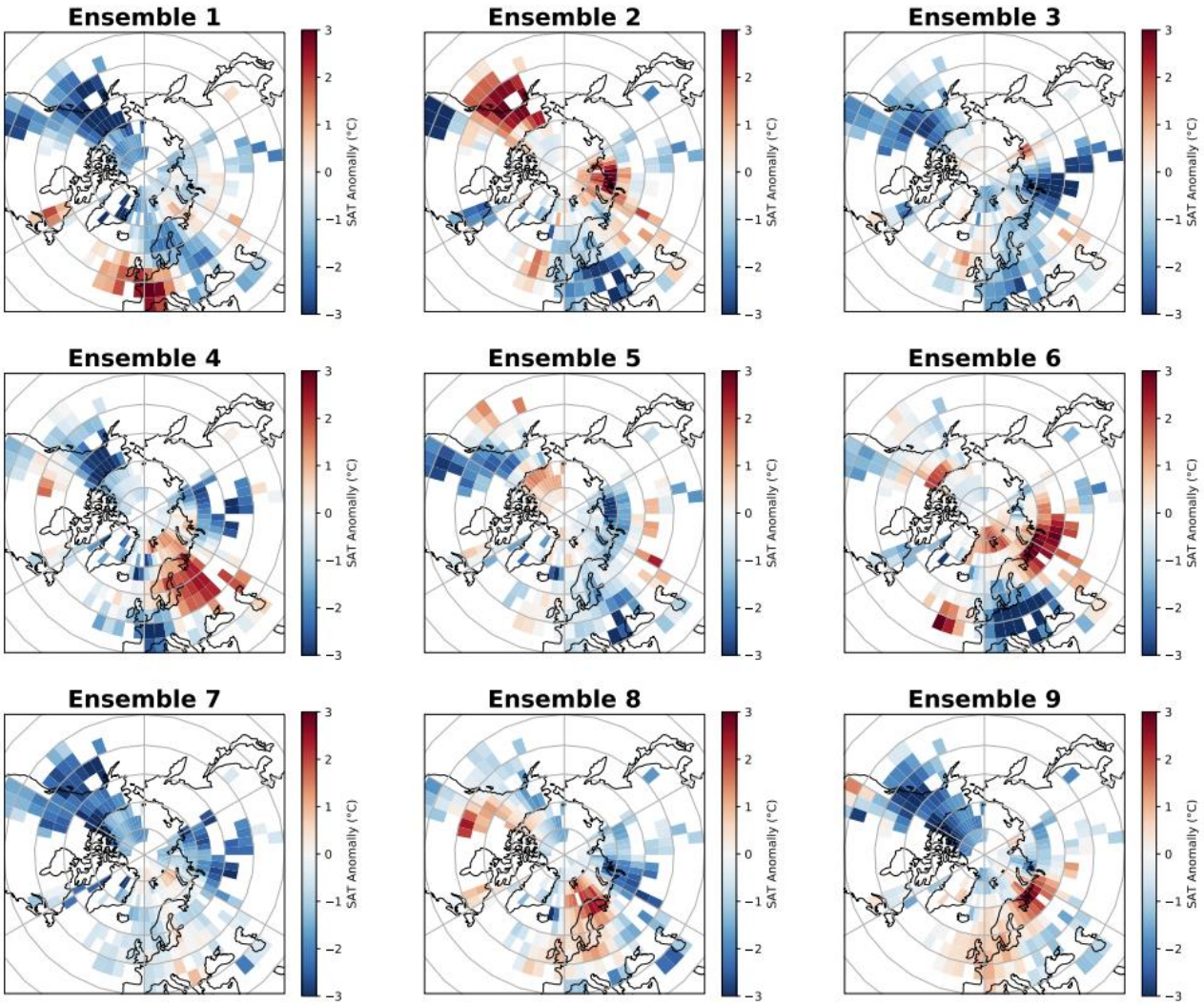

Figure S6. Spatially resolved NH Summer (JJA) Temperature Anomalies for individual July 1257 ensembles for Summer 1259. Model-simulated anomalies were regridded to be comparable to the NTREND spatially resolved dataset (Anchukaitis et al., 2017).

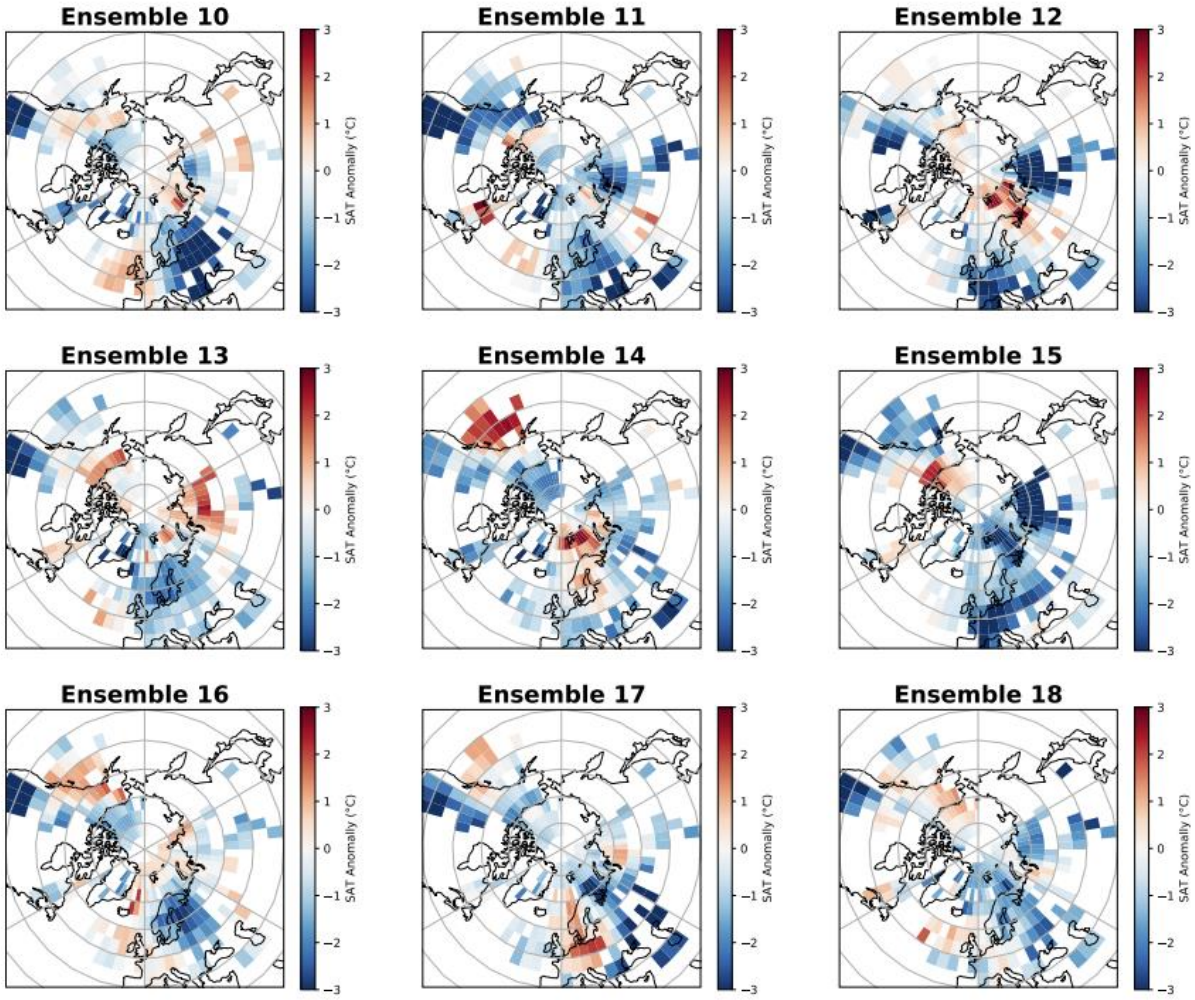

Figure S7. Spatially resolved NH Summer (JJA) Temperature Anomalies for individual January 1258 ensembles for Summer 1259. Model-simulated anomalies were regridded to be comparable to the NTREND spatially resolved dataset (Anchukaitis et al., 2017).

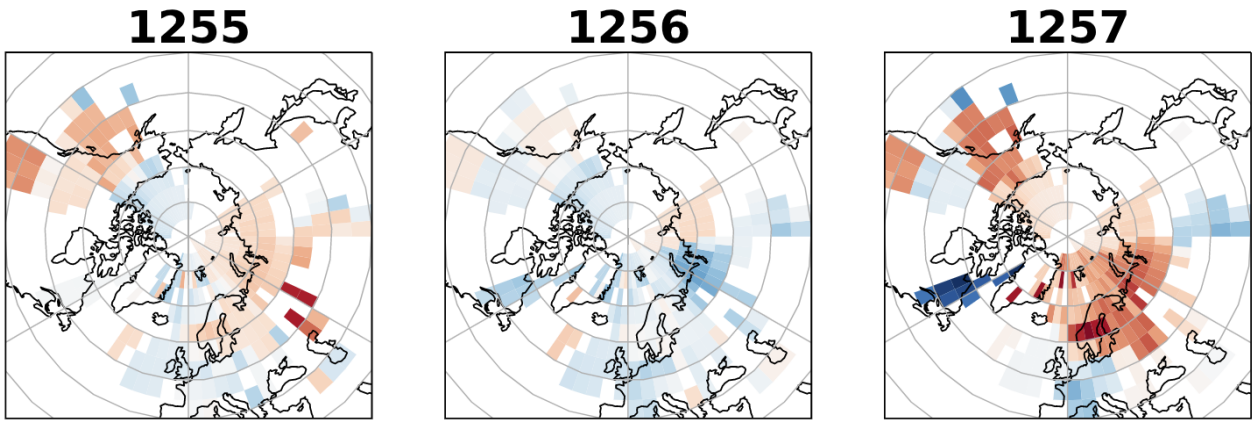

Figure S8. NTREND NH Summer (JJA) Tree Ring-reconstructed SAT reconstructions 1255-1257 (Anchukaitis et al., 2017). Moderate positive SAT anomalies are present in Alaska and the US West Coast in 1255 with the onset of strong positive SAT anomalies occurring in 1257. This may be indicative of prevailing warm phase El Nino-like conditions in 1257 prior to the Mt Samalas Eruption.

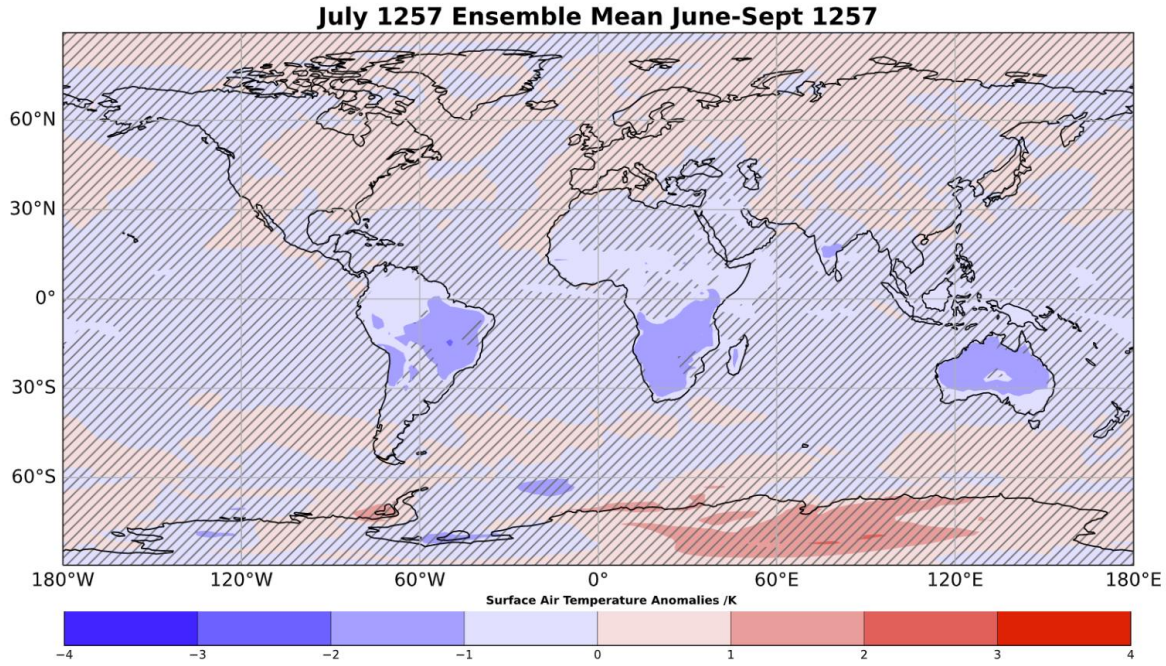

Figure S9: Model-simulated surface air temperature anomalies averaged for June-Sept 1257 for a July 1257 eruption. Hashed lines denote regions of < 95% significance as determined by a grid point ANOVA test. Only Significant negative anomalies are only seen over the continents in the Southern Hemisphere of up to -2°C. No negative anomalies occur at >95% significance along the West Coast of the US or Canada.

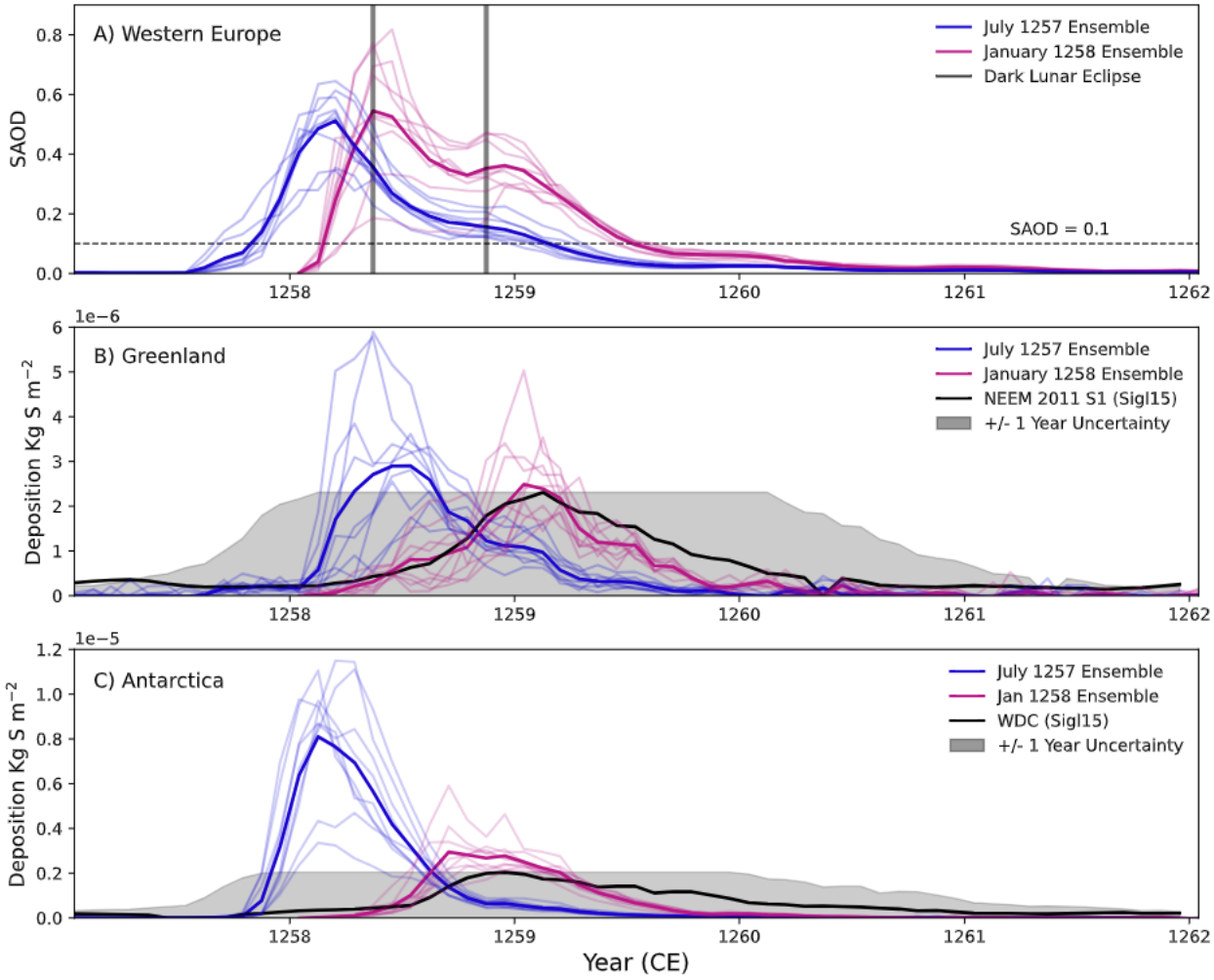

Figure S10: A) Model-simulated Stratospheric Aerosol Optical Depth (SAOD) timeseries over Western Europe (Lat: 40-60°N, Longitude: 10W-10°E) for July 1257 (blue line) and Jan 1258 (pink line) eruption scenarios where bold lines are the ensemble means. Vertical grey bars denote historical records of dark lunar eclipses in May 1258 (England) and November 1258 (Genoa). The dashed horizontal line at SAOD = 0.1 denotes the minimum SAOD required for a dark lunar eclipse. B-C) Model-simulated S deposition ice sheet averages over Greenland and Antarctica for July 1257 (Blue) and January 1258 (Pink) eruption scenarios. Black lines are timeseries from NEEM (Greenland) and WDC (Antarctica) ice core records respectively (Sigl et al., 2015) with grey shading showing +/- 1-year temporal uncertainty for those records.

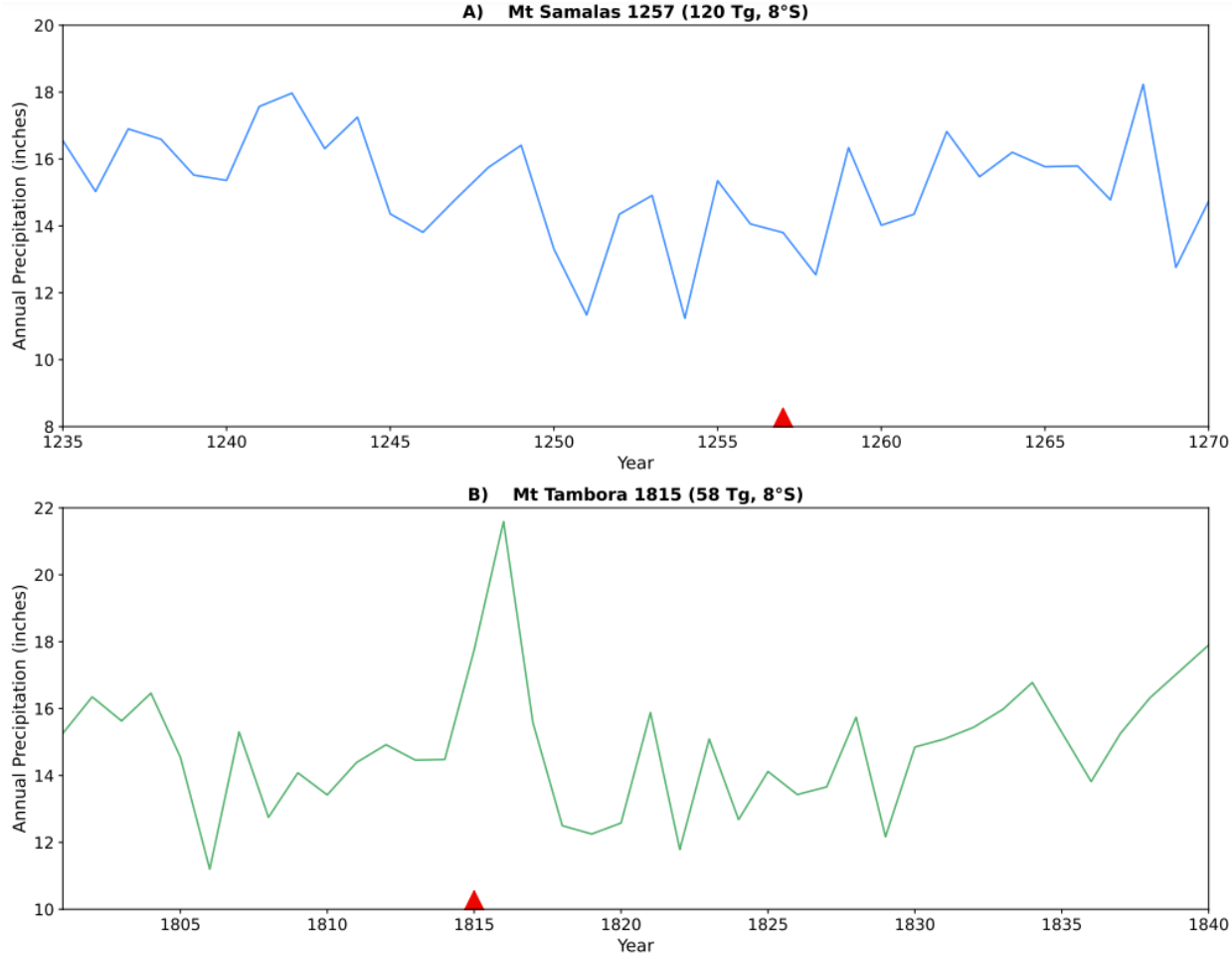

Figure S11. Tree-ring reconstructed annual precipitation for El Malpais, New Mexico. Panel A shows reconstructions between 1235-1270 with the Mt Samalas eruption (red triangle) occurring in 1257. No large perturbation to annual precipitation is seen in the years following the eruption. Panel B shows reconstructions from 1800-1840 with the Mt Tambora eruption (red triangle) occurring in 1815. A large positive perturbation (increased rainfall) is seen following the eruption potentially indicative of a latitudinal ITCZ shift.

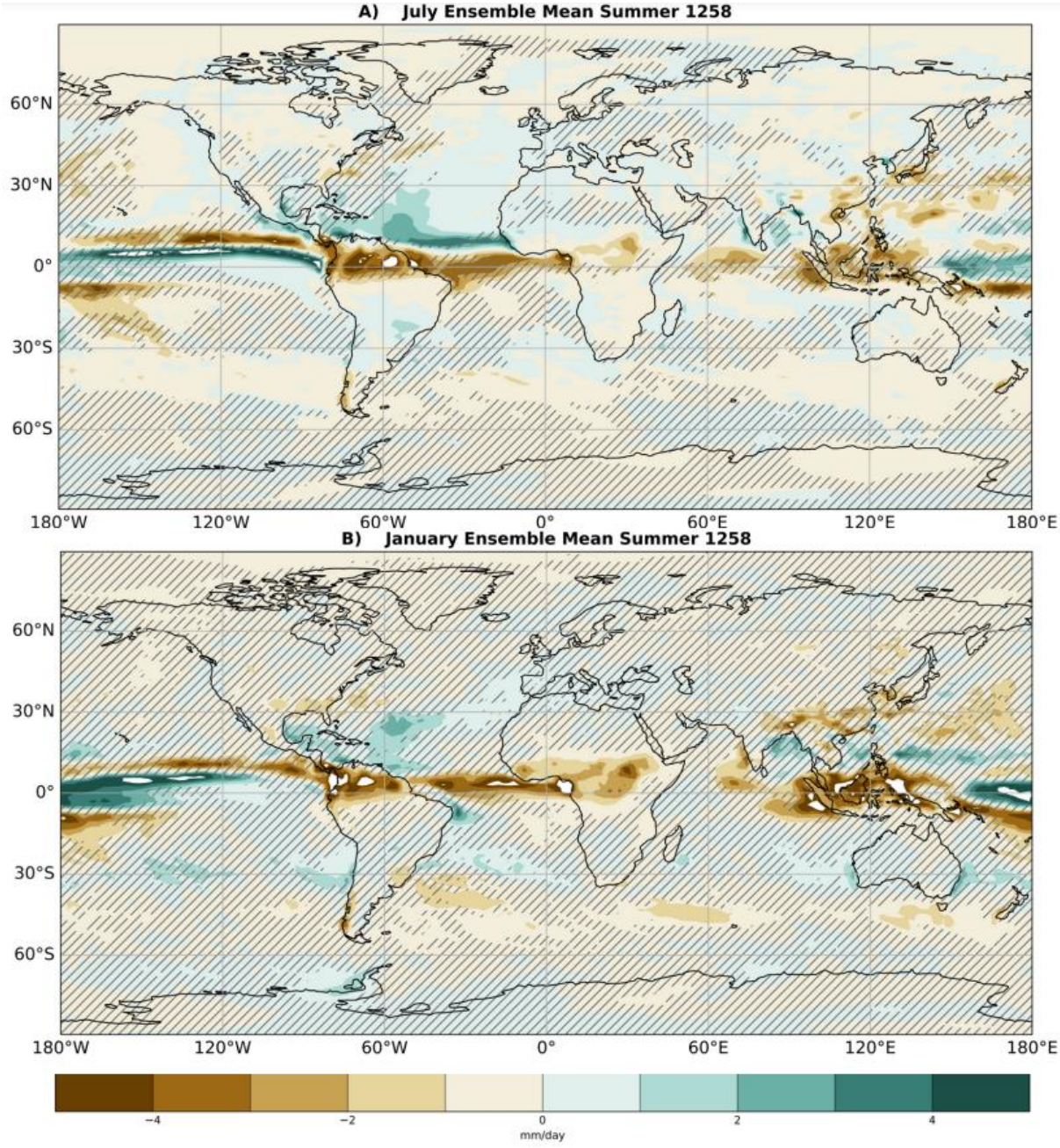

Figure S12. Globally resolved NH Summer (JJA) Precipitation Anomalies for the July 1257 ensemble mean (Top) and the January 1258 ensemble mean (Bottom) for Summer 1258. Hashed lines denote anomalies at <95% significance as determined by a grid point ANOVA analysis.